Water Research 221 (2022) 118794

Contents lists available at ScienceDirect

Water Research

journal homepage: www.elsevier.com/locate/watres

Micropollutant degradation by UV/H_2O_2 in drinking water: Facilitated prediction through combination of model simulation and portable measurement

Yanyan Huang [a,b], Zhimin Qiang [a,b,*], Zhe Sun [a], Mengkai Li [a,b,*]

[a] Key Laboratory of Drinking Water Science and Technology, Research Center for Eco-Environmental Sciences, Chinese Academy of Sciences, 18 Shuang-qing Road, Beijing 100085, China
[b] University of Chinese Academy of Sciences, 19 Yu-quan Road, Beijing 100049, China

ARTICLE INFO

Keywords:
UV/H_2O_2
Micropollutant degradation
Model simulation
Portable measurement
Facilitated prediction method

ABSTRACT

Ultraviolet-based advanced oxidation processes (UV-AOPs) are highly effective for micropollutant degradation. However, it is considerably time and labor consuming to evaluate the practical performance of UV-AOPs. This study developed a novel method, through combination of model simulation with portable measurement (MS-PM), to facilitate prediction of the photon fluence-based rate constant of micropollutant degradation ($k'_{p,MP}$) by UV/H_2O_2, a commercially available UV-AOP. Model simulation was performed with photochemical, hydroxyl radical ($HO^{\bullet}$) concentration steady-state approximation, and quantitative structure-activity relationship models; and portable measurement was conducted on a mini-fluidic photoreaction system to quantify the $HO^{\bullet}$ scavenging capacity (HRSC) of a water matrix. The method was established and further verified experimentally in seven test waters by taking sulfamethazine (SMN) as a model micropollutant. A lower $k'_{p,SMN}$ was predicted in a water matrix with a higher HRSC, for example, 57.5 and 347.8 m^2 $einstein^{-1}$ in the raw water (HRSC = 5.91×10^5 s^{-1}) and sand-filtered effluent (HRSC = 5.25×10^4 s^{-1}) of a drinking water treatment plant at an H_2O_2 dose of 25 mg L^{-1}, respectively. The predicted values agreed generally well with the experimental ones. The MS-PM method has advantages of high efficiency and convenience, low cost, and acceptable accuracy, which will significantly facilitate the design and field assessment of UV-AOPs for micropollutant removal from drinking water.

Abbreviations

a: absorption coefficient at 254 nm [cm^{-1}]
DBE: double bond equivalence
DOC: dissolved organic carbon [mg L^{-1}]
DOM: dissolved organic matter
E_{HOMO}: energy of the highest occupied molecular orbital [eV]
$E^0_{p,UV}$: UV photon fluence rate [einstein m^{-2} s^{-1}]
f: UV photon absorption fraction
$F^0_{p,UV}$: UV photon fluence [einstein m^{-2}]
h_{tube}: length of UV tube [m]
HA: humic acid
HLG: energy difference between the highest occupied and lowest unoccupied molecular orbitals [eV]
$HO^{\bullet}$: hydroxyl radical
$[HO^{\bullet}]_{ss}$: steady-state concentration of hydroxyl radical [mg L^{-1}]
HRSC: hydroxyl radical scavenging capacity [s^{-1}]
IPA: isopropyl alcohol
k': photon fluence-based rate constant of micropollutant degradation [m^2 $einstein^{-1}$]
$k_{HO\bullet}$: second-order rate constant for the reaction with hydroxyl radical [M^{-1} s^{-1}]
l': effective optical path-length of photoreactor [cm]
MB: methylene blue
MFPS: mini-fluidic photoreaction system
MLR: multiple linear regression
MS-PM: model simulation with portable measurement
PCA: principal component analysis
p-CBA: *para*-chlorobenzoic acid
PFS/UF: polymeric ferric sulfate coagulation/ultrafiltration effluent

* Corresponding authors at: Key Laboratory of Drinking Water Science and Technology, Research Center for Eco-Environmental Sciences, Chinese Academy of Sciences, 18 Shuang-qing Road, Beijing 100085, China.
E-mail addresses: qiangz@rcees.ac.cn (Z. Qiang), mkli@rcees.ac.cn (M. Li).

https://doi.org/10.1016/j.watres.2022.118794
Received 10 January 2022; Received in revised form 18 June 2022; Accepted 24 June 2022
Available online 25 June 2022

Φ: quantum yield at 254 nm [mole einstein^{-1}]
q_0: incident UV photon flux [einstein s^{-1}]
Q^2_{Ext}: external explained variance
Q^2_{LOO}: leave-one-out cross-validation
QSAR: quantitative structure-activity relationship
r: pearson correlation coefficient
$r_{HO•}$: formation rate of hydroxyl radical [M s^{-1}]
r_{tube}: internal radius of UV tube [m]
R^2: correlation coefficient
RE: relative error
RPDs: relative percent differences
RW: raw water
SF: sand-filtered effluent
SMC: surrogate matrix component
SMN: sulfamethazine
SSA: steady-state approximation
SW: synthetic water
t: total reaction time [s]
t_{ree}: reduction equivalent exposure time [s]
UP: ultrapure water
UPLC-MS/MS: ultra-high performance liquid chromatograph-tandem mass spectrometer
UV-AOPs: ultraviolet-based advanced oxidation processes
V: total volume of reaction solution [L]
#acid: number of carboxylic acid groups
#C: number of carbon atoms
#H: number of hydrogen atoms
#nonHatoms: number of non-hydrogen atoms
#O:C: oxygen to carbon ratio
#ringatoms: number of ring atoms

1. Introduction

Micropollutants, such as antibiotics and endocrine disrupting chemicals, have raised great concerns because of their harmful impacts on ecological safety and human health even at trace concentrations (Schwarzenbach et al., 2006). Conventional water treatment processes (e.g., coagulation/sedimentation, filtration, and disinfection) cannot effectively remove micropollutants. In recent years, ultraviolet-based advanced oxidation processes (UV-AOPs) have drawn increasing attention because they can produce highly reactive radicals to quickly degrade most micropollutants (Lester et al., 2014; Yang et al., 2016; Lee et al., 2020). Among them, UV/H_2O_2 is the most commonly applied process because of its high quantum yield of hydroxyl radical (HO$^•$), easy operation, small footprint, and no secondary pollution (Wunsch et al., 2021).

To evaluate the performance of UV-AOPs for process design and field inspection, it is necessary to determine the micropollutant degradation kinetics. Because UV reactors of different configurations deliver different fluence rates, the photon fluence-based rate constant of micropollutant degradation ($k'_{p,MP}$, m^2 einstein^{-1}) has been more commonly adopted for UV-AOPs than the time-based rate constant (s^{-1}) for the purpose of result comparison among different laboratories (Rosenfeldt and Linden, 2007; Bolton et al., 2015). The $k'_{p,MP}$ is affected by many factors such as oxidants, micropollutants, water matrices, and operating parameters. Hence, numerous experiments should be conducted to determine the optimal process and operation conditions as well for a desired removal efficiency of target micropollutants. This requires frequent field water collections/transportations, various bench-scale tests using a well-established photoreactor, and high professional skills for operation of the photoreactor (e.g., *quasi*-collimated beam apparatus) and advanced analytical instruments (e.g., an ultra-high performance liquid chromatograph-tandem mass spectrometer (UPLC-MS/MS) for micropollutant analysis), which is considerably time and labor consuming and thus expensive. Therefore, there is an urgent need to develop a method for facilitated prediction of the $k'_{p,MP}$ under practical operation conditions of UV-AOPs.

The photochemical model and HO$^•$ concentration steady-state approximation (SSA) model have been applied to kinetic simulations of micropollutant degradation by UV/H_2O_2 (Glaze et al., 1995; Baeza and Knappe, 2011). The direct UV photolysis rate constant and the steady-state HO$^•$ concentration (i.e., $[HO^•]_{ss}$) can be estimated through model simulations, and then the indirect oxidation rate constant via HO$^•$ is calculated as the product of $[HO^•]_{ss}$ and the second-order reaction rate constant of a target micropollutant toward HO$^•$ ($k_{HO•,MP}$). The $k_{HO•,MP}$ can be obtained from published literatures, measured experimentally by competition kinetics method (Onstein et al., 1999), or predicted by a quantitative structure-activity relationship (QSAR) model (Lee and von Gunten, 2012; Sudhakaran and Amy, 2013).

However, the prediction of $k'_{p,MP}$ in real waters is a complex issue because the water matrix such as dissolved organic matter (DOM) and inorganic ions (e.g., HCO_3^-/CO_3^{2-}, NO_3^-, and PO_4^{3-}) will compete against the target micropollutant for reactive radicals formed during the UV/H_2O_2 process (Kwon et al., 2019). It is usually impossible to analyze all water matrix components and their concentrations required for the model input, which may induce a large error in the $k'_{p,MP}$ prediction. Fortunately, an integrated index, HO$^•$ scavenging capacity (HRSC), has been recently proposed to represent the overall HO$^•$ competitiveness of a water matrix, which can be easily measured by a visible spectrophotometer (Wang et al., 2020). Furthermore, we have previously developed a mini-fluidic photoreaction system (MFPS) to facilitate bench-scale photochemical studies. Compared to the commonly used *quasi*-collimated beam apparatus, the MFPS has obvious advantages such as output of a high photon fluence rate to greatly reduce the experimental time, accurate determination of photon fluence by using a micro fluorescent silica detector to monitor the real-time fluctuation of lamp output, on-line absorbance measurement, photoreactor temperature control, and a small size (Li et al., 2016a). Therefore, it is an ideal portable device for field measurement of the HRSC of a real water matrix.

This study was aimed to develop a new method, through combination of model simulation with portable measurement (MS-PM), to facilitate the prediction of micropollutant degradation by UV/H_2O_2. The model simulation was performed with photochemical, HO$^•$ concentration SSA, and QSAR models; and the portable measurement was conducted on the MFPS to quantify the HRSC of a water matrix. Sulfamethazine (SMN), a typical sulfonamide antibiotic frequently detected in various waters (Hou et al., 2015; Chen et al., 2020), was selected as a model micropollutant. The photon fluence-based degradation rate constants of SMN by UV/H_2O_2 (i.e., $k'_{p,SMN}$) were predicted by the MS-PM method in seven test waters and further verified experimentally. The novel method is expected to significantly facilitate the design and field assessment of UV-AOPs for micropollutant removal from drinking water.

2. Materials and methods

2.1. Chemicals and analytical methods

All chemicals used were of at least reagent grade. Hydrogen peroxide (H_2O_2), isopropyl alcohol (IPA) and sodium bisulfite ($NaHSO_3$) were purchased from Sinopharm Chemical Reagent Co. (China); *para*-chlorobenzoic acid (*p*-CBA), humic acid (HA), methylene blue (MB) and uridine from Sigma-Aldrich (USA); SMN from Thermo Fisher Scientific (USA); and titanium (IV) oxy-sulfate ($TiOSO_4$) from Fluka (Germany).

SMN was detected with UPLC-MS/MS (Agilent 1290 Infinity UPLC and 6420 Triple Quad LC/MS, USA) coupled with a Zorbax SB-C18 column (100 mm × 2.1 mm, 1.8 μm particle size) after the residual H_2O_2 in water samples was quenched with an excess of $NaHSO_3$. H_2O_2 was analyzed by the $TiOSO_4$ method (Eaton et al., 1995). MB was analyzed on an online DR1900 spectrophotometer (Hach, USA) at 664 nm. Uridine and UV_{254} were analyzed on a UV-2600 spectrophotometer

(Shimadzu, Japan) at 262 and 254 nm, respectively. Dissolved organic carbon (DOC) and ferric ion (Fe^{3+}) were measured by a total organic carbon analyzer (TOC-VCPH/CPN, Shimadzu, Japan) and an inductively coupled plasma optical emission spectrometer (ICP-OES, Optima 2000, PerkinElmer, USA), respectively. All reaction solutions were prepared with ultrapure water (UP) produced from a Milli-Q system (Advantage A10, Millipore, USA). All experiments were conducted at least twice.

2.2. Simulation models

2.2.1. Photochemical model

In the UV/H_2O_2 process, micropollutant degradation results from both direct UV photolysis and indirect oxidation via $HO^{\bullet}$, which is expressed as follows:

$$k'_{p,MP} = k'_{d,MP} + k'_{i,MP} \quad (1)$$

$$k'_{d,MP} = \frac{\Phi_{MP} q_0 f_{MP} \left(1 - 10^{-al'}\right)}{V E^0_{p,UV}[MP]} \quad (2)$$

where $k'_{d,MP}$ and $k'_{i,MP}$ = photon fluence-based pseudo-first-order rate constants of micropollutant degradation by direct photolysis and indirect oxidation (m^2 $einstein^{-1}$), respectively; Φ_{MP} = quantum yield of direct photolysis of micropollutant (mole $einstein^{-1}$); q_0 = incident UV photon flux (einstein s^{-1}); f_{MP} = UV photon absorption fraction of micropollutant; V = total volume of reaction solution (L); a = absorption coefficient of test solution (cm^{-1}); l' = effective optical path-length of photoreactor (cm); and $E^0_{p,UV}$ = UV photon fluence rate (einstein m^{-2} s^{-1}).

The dominant reactive radical is $HO^{\bullet}$ in the UV/H_2O_2 process, whose formation rate ($r_{HO^{\bullet}}$, M s^{-1}) can be expressed by Eq. (3):

$$r_{HO^{\bullet}} = \frac{\Phi_{H_2O_2} q_0 f_{H_2O_2} \left(1 - 10^{-al'}\right)}{V} \quad (3)$$

where $\Phi_{H_2O_2}$ = quantum yield of $HO^{\bullet}$ (1.11 mole $einstein^{-1}$) (Goldstein et al., 2007); and $f_{H_2O_2}$ = UV photon absorption fraction of H_2O_2.

2.2.2. SSA model

The SSA model applied to the UV/H_2O_2 process assumes that the rate of $HO^{\bullet}$ consumption by water matrix, target micropollutant, and H_2O_2 is equal to its formation rate, so the $HO^{\bullet}$ concentration reaches approximately steady state (i.e., $[HO^{\bullet}]_{ss}$). Hence, the $[HO^{\bullet}]_{ss}$ and $k'_{i,MP}$ can be calculated consecutively as follows:

$$[HO^{\bullet}]_{ss} = \frac{r_{HO^{\bullet}}}{\sum k_{HO^{\bullet},S_i}[S_i] + k_{HO^{\bullet},MP}[MP] + k_{HO^{\bullet},H_2O_2}[H_2O_2]} \quad (4)$$

$$k'_{i,MP} = \frac{k_{HO^{\bullet},MP}[HO^{\bullet}]_{ss}}{E^0_{p,UV}} \quad (5)$$

where $[S_i]$ = concentration of a water matrix component (S_i) (M); $k_{HO^{\bullet},S_i}$ = second-order reaction rate constant of S_i with $HO^{\bullet}$ (M^{-1} s^{-1}); $\sum k_{HO^{\bullet},S_i}[S_i]$ = HRSC of a water matrix (s^{-1}); and $k_{HO^{\bullet},MP}$ and $k_{HO^{\bullet},H_2O_2}$ = second-order reaction rate constants of a micropollutant and H_2O_2 with $HO^{\bullet}$, respectively. The $k_{HO^{\bullet},H_2O_2}$ was reported to be 2.7×10^7 M^{-1} s^{-1} (Grebel et al., 2010).

2.2.3. QSAR model

QSAR model was used to predict the $k_{HO^{\bullet},MP}$ of a target micropollutant. A data set consisting of 50 organic compounds with known second-order reaction rate constants with $HO^{\bullet}$ ($k_{HO^{\bullet},OC}$) was established, which was further divided into a training set and a validation set with a ratio of the number of organic compounds being 4:1 (Luo et al., 2019). These organic compounds containing various functional groups cover a wide structural diversity to ensure the representativeness and broad applicability of the established QSAR model (Sudhakaran and Amy, 2013; Xiao et al., 2015). For each organic compound, totally 19 descriptors reflecting the constitutional, electrostatic and quantum chemical properties were examined, which were reported pertinent to radical reactivity (Kusic et al., 2009; Luo et al., 2017). The molecular structure of each compound was preliminarily obtained by ChemBio3D Ultra 12.0, and optimized by the B3LYP function, 6-31+G(d,p) basis set and polarizable continuum model (taking account of the solvent effect of water) of Gaussian 09 to achieve the local minimum-energy conformation (Lee et al., 2015; Borhani et al., 2016).

Then, by using SPSS 19.0, Pearson correlation analysis and principal component analysis (PCA) were performed to screen out the significant descriptors, and a linear relationship (i.e., QSAR model) between $\ln k_{HO^{\bullet},OC}$ and the most significant descriptors was established through stepwise multiple linear regression (MLR) (Sudhakaran and Amy, 2013; Jin et al., 2015). The QSAR model was further assessed by correlation coefficient (R^2), leave-one-out cross-validation (Q^2_{LOO}), and external explained variance (Q^2_{Ext}), as detailed in Text S1. Finally, the second-order reaction rate constant of a target micropollutant with $HO^{\bullet}$ (e.g., $k_{HO^{\bullet},SMN}$) could be readily predicted by the QSAR model established.

2.3. Portable measurement of HRSC

2.3.1. Measurement device

The MFPS developed previously was used to measure the HRSC of a water matrix after certain modification. Its core part was a photoreactor containing an 8 W low-pressure mercury vapor lamp (Wanhua Co., Zhejiang, China) as the light source and a straight quartz tube for UV exposure (Fig. S1). The photoreactor was featured with a portable size (ca. 4 cm of outer diameter and 30 cm of length) and a light weight (ca. 200 g). Reaction solution stored in a glass container under magnetic stirring was recirculated with a peristaltic pump sequentially through the UV tube and an on-line portable spectrophotometer (Hach DR1900). Because only a part of the reaction solution could receive the UV exposure during each circulation, a reduction equivalent exposure time (t_{ree}, s) was defined as the total reaction time (t, s) multiplied by the ratio of the exposure volume of the UV tube ($\pi r^2_{tube} h_{tube}$, m^3) to the total volume of the reaction solution (V, m^3):

$$t_{ree} = \frac{\pi r^2_{tube} h_{tube}}{V} t \quad (6)$$

where r_{tube} and h_{tube} = internal radius (0.13 cm) and length (29 cm) of the UV tube, respectively.

The UV photon fluence ($F^0_{p,UV}$, einstein m^{-2}) can then be calculated by Eq. (7):

$$F^0_{p,UV} = E^0_{p,UV} t_{ree} \quad (7)$$

The $E^0_{p,UV}$ in the UV tube was determined to be 3.98×10^{-4} einstein m^{-2} s^{-1} with a uridine solution (0.012 mM), as shown in Fig. S2 (Jin et al., 2006).

2.3.2. Measurement procedures

As mentioned above, the HRSC (i.e., $\sum k_{HO^{\bullet},S_i}[S_i]$ in Eq. (4)) was defined to represent the overall capacity of a water matrix competing for $HO^{\bullet}$ in this study. The HRSC measurement procedures are illustrated in Fig. 1. Specifically, MB was used as a probe, and IPA (or *p*-CBA) was used as a surrogate matrix component (SMC). A series of standard solutions were prepared with MB (5.0 mg L^{-1}) and SMC with different concentrations ($[IPA]_0$ = 0–320 μM, or $[p\text{-CBA}]_0$ = 0–20 μM) to represent different HRSCs. Because the direct UV photolysis of MB (Fig. S3) and IPA/*p*-CBA was negligible (Rosenfeldt and Linden, 2007; Wu et al., 2008), these compounds were degraded predominantly by $HO^{\bullet}$ formed in the UV/H_2O_2 process. Hence, the rearrangement of Eqs. (4) and (5) yields a linear relationship between $1/k'_{p,MB}$ and HRSC (i.e., standard curve):

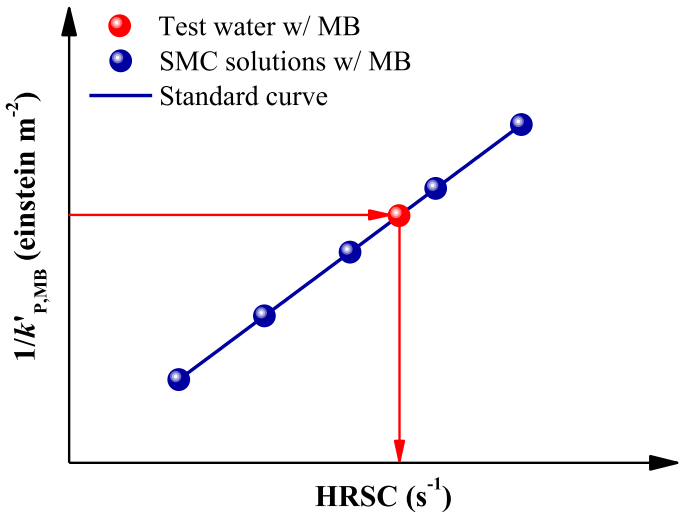

Fig. 1. Schematic diagram of HRSC measurement procedures.

$$1/k'_{p,MB} = \frac{E^0_{P,UV}}{k_{HO^\bullet,MB} r_{HO^\bullet}} HRSC + \frac{E^0_{P,UV}\left(k_{HO^\bullet,MB}[MB] + k_{HO^\bullet,H_2O_2}[H_2O_2]\right)}{k_{HO^\bullet,MB} r_{HO^\bullet}} \quad (8)$$

where $k'_{p,MB}$ = photon fluence-based pseudo-first-order rate constant of MB degradation (m^2 einstein^{-1}), as measured with the MFPS; and $k_{HO^\bullet,MB}$ = second-order reaction rate constant of MB with HO$^\bullet$ (2.1×10^{10} M^{-1} s^{-1}) (Buxton et al., 1988).

The HRSC of a standard solution was calculated as the product of the second-order reaction rate constant of an SMC (i.e., IPA/*p*-CBA) and its spiked concentration. The $k_{HO^\bullet,IPA}$ and $k_{HO^\bullet,p\text{-}CBA}$ were reported to be 1.9×10^9 and 5.0×10^9 M^{-1} s^{-1}, respectively (Buxton et al., 1988). As different HRSCs resulted in different $k'_{p,MB}$ values, a standard curve could be established through linear regression (i.e., Eq. (8)). Thereafter, by spiking MB (5.0 mg L^{-1}) into a test water and measuring the $k'_{p,MB}$ in the UV/H_2O_2 process with the MFPS, the HRSC of the test water could be obtained by referring to the standard curve (Fig. 1).

2.4. MS-PM method

By combining the model simulation with the portable measurement as aforementioned, the MS-PM method was developed to facilitate the prediction of micropollutant degradation (i.e., $k'_{p,MP}$) in the UV/H_2O_2 process. The prediction procedures of this method for a target micropollutant are summarized in Fig. 2: (1) calculate the $k'_{d,MP}$ using the photochemical model of direct UV photolysis (i.e., Eq. (2)); (2) calculate the $r_{HO^\bullet}$ using the photochemical model of HO$^\bullet$ formation rate (i.e., Eq. (3)) and the $k_{HO^\bullet,MP}$ using the QSAR model developed; (3) establish a standard curve (i.e., a plot of $1/k'_{p,MB}$ vs. HRSC) in laboratory; (4) measure the $k'_{p,MB}$ in a test water with the MFPS in field, and obtain the HRSC of the test water by referring to the standard curve; (5) calculate the $[HO^\bullet]_{ss}$ using the SSA model (i.e., Eq. (4)) and the $k'_{i,MP}$ using Eq. (5); and (6) obtain the $k'_{p,MP}$ by summing up the $k'_{d,MP}$ and $k'_{i,MP}$ (i.e., Eq. (1)).

2.5. Test waters

Seven different types of waters were tested, including a UP, two synthetic waters prepared by dissolving HA in the UP with DOC values of 1.02 (SW1) and 5.00 mg L^{-1} (SW2), a raw water (RW1) and a sand-filtered effluent (SF) collected from a drinking water treatment plant located in Yancheng City of Jiangsu Province, and a raw water (RW2) and a polymeric ferric sulfate coagulation/ultrafiltration effluent (PFS/UF) collected from a rural drinking water treatment facility located in Changzhou City of Jiangsu Province. The major quality parameters of these waters are provided in Table 1. All test waters were filtered through 0.45 μm membrane filters and stored in a refrigerator (4 ℃) before experiments.

Table 1
Major quality parameters of seven test waters.

Test water	pH	UV_{254} (cm^{-1})	DOC (mg L^{-1})	Fe^{3+} (mg L^{-1})
UP	6.50	0.000	0.00	0.00
SW1	6.28	0.029	1.02	0.00
SW2	7.10	0.120	5.00	0.00
RW1	8.15	0.123	5.91	0.04
SF	7.85	0.080	3.87	0.06
RW2	7.71	0.137	6.10	0.05
PFS/UF	8.00	0.104	3.89	0.34

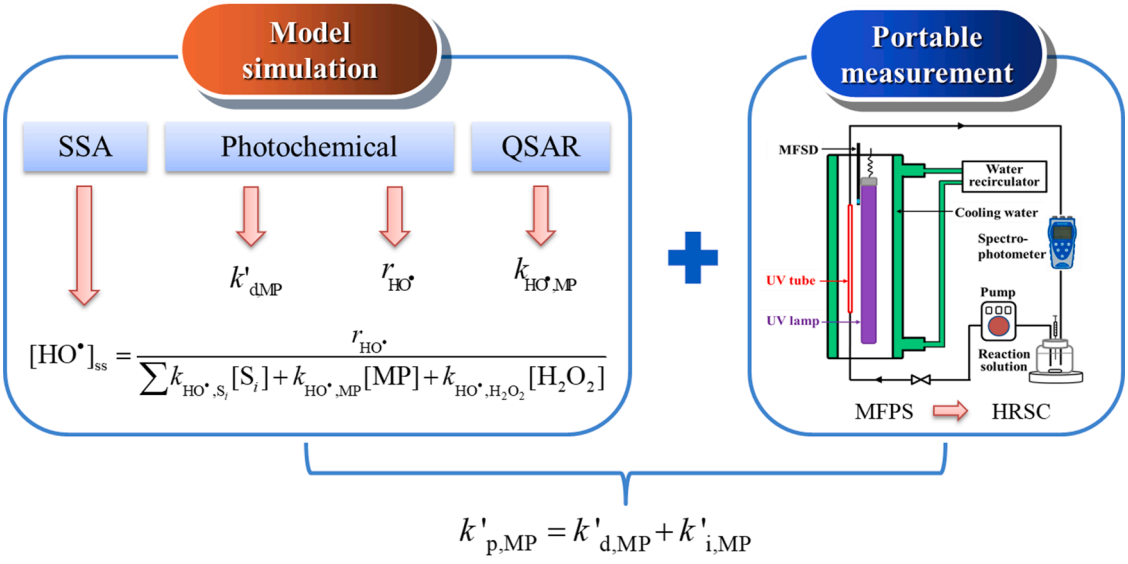

Fig. 2. Schematic diagram of prediction procedures of MS-PM method.

3. Results

3.1. Prediction of $k'_{d,SMN}$ and $r_{HO\bullet}$ by photochemical model

Taking SMN as a model micropollutant, its photon fluence-based degradation rate constant via direct UV photolysis (i.e., $k'_{d,SMN}$) in the UV/H_2O_2 process could be predicted by Eq. (2) at different initial concentrations of H_2O_2 ($[H_2O_2]_0$) and SMN ($[SMN]_0$). As shown in Table S1, the $k'_{d,SMN}$ varied little in the range of 19.26−19.44 m^2 einstein^{-1} at $[H_2O_2]_0$ = 5–25 mg L^{-1} and $[SMN]_0$ = 0.010−100 μg L^{-1}, which was due to the low quantum yield of SMN under direct UV photolysis (Φ_{SMN} = 0.005 mole einstein^{-1}) as well as the small photon absorption coefficients of H_2O_2 ($a_{H_2O_2} \leq 0.014$ cm^{-1}) and SMN ($a_{SMN} \leq 0.006$ cm^{-1}) under the experimental conditions applied (Boreen et al., 2005; Wang et al., 2012). By using the photochemical model of HO$^\bullet$ formation rate (i.e., Eq. (3)), the $r_{HO\bullet}$ in the UV/H_2O_2 process could be predicted at different $[H_2O_2]_0$ and $[SMN]_0$ values. As shown in Fig. S4, the predicted $r_{HO\bullet}$ exhibited a linear relationship with $[H_2O_2]_0$ in the range of 5–25 mg L^{-1}, but was almost independent of $[SMN]_0$ in the range of 0.010−100 μg L^{-1}.

3.2. QSAR model establishment and prediction of $k_{HO\bullet,SMN}$

To establish the QSAR model, 19 descriptors were initially selected, which are pertinent to the radical reactivity and thus frequently used to predict the second-order reaction rate constants of organic compounds (Xiao et al., 2015; Li et al., 2019). Afterwards, Pearson correlation analysis, PCA and stepwise MLR were successively performed to reduce the dimensionality of variables in the training set (40 organic compounds).

First, Pearson correlation analysis was performed between the $\ln k_{HO\bullet,OC}$ and each descriptor, and 9 descriptors (i.e., #C, #H, #O:C, #acid, #ringatoms, #nonHatoms, DBE, E_{HOMO}, and HLG) were screened out with an absolute Pearson correlation coefficient ($|r|$) > 0.4 at the 0.01 significance level (double tailed) (Table S2). Second, PCA was performed to screen out significant descriptors. As shown in Fig. S5, the first three components accounted for 90.4% of the total variance. The component loading plots further reveal that #C, #acid and E_{HOMO} had the highest loading score in Components 1, 2 and 3, respectively (Fig. S6). E_{HOMO} represents the electron donating ability of a molecule, which has been reported closely pertinent to the reactivity towards HO$^\bullet$ (Wang et al., 2009; Luo et al., 2017). In addition, #O:C and HLG were also selected because they had the second highest loading score (absolute value) in Components 2 and 3, respectively, and did not cluster with other descriptors. Finally, the stepwise MLR was performed to establish the QSAR model, which also identified the two most significant descriptors (i.e., #O:C and E_{HOMO}). Table 2 shows three equations which established the linear relationship between the $\ln k_{HO\bullet,OC}$ and one, two and five descriptors screened out above, respectively. By comparing the values of R^2, Q^2_{LOO} and Q^2_{Ext} (Text S1) and considering the conciseness in expression, the QSAR model was established as follows:

$$\ln k_{HO\bullet,OC} = 27.992 - 2.131 \times (\#O:C) + 0.772 \times E_{HOMO} \quad (9)$$

Table S3 lists the values of #O:C and E_{HOMO} involved in the QSAR model as well as the literature and predicted $k_{HO\bullet,OC}$ values of each organic compound in the entire data set. For most organic compounds, the predicted $k_{HO\bullet,OC}$ values agreed fairly well with the literature ones (Fig. 3), while the largest deviation of $k_{HO\bullet,OC}$ (about 10-fold) was observed for lactate (Table S3). It is worth noting that in respect to the second-order reaction rate constant of an organic compound with a reactive radical, the accuracy of a QSAR model is usually considered acceptable if the predicted value deviates from the measured one within one order of magnitude (Kusic et al., 2009; Xiao et al., 2015). By using the established QSAR model (i.e., Eq. (9)), $k_{HO\bullet,SMN}$ was readily predicted to be 7.2 × 10^9 M^{-1} s^{-1}, which is quite close to those reported before ((5.0 ± 0.3) × 10^9 M^{-1} s^{-1}, Boreen et al., 2005; (8.3 ± 0.8) × 10^9 M^{-1} s^{-1}, Mezyk et al., 2007).

Table 2
Establishment of QSAR model.

No.	Equation	R^2	Q^2_{LOO}	Q^2_{Ext}
1	$\ln k_{HO\bullet,OC} = 22.899 - 2.434 \times (\#O:C)$	0.57	0.44	0.65
2	$\ln k_{HO\bullet,OC} = 27.992 - 2.131 \times (\#O:C) + 0.772 \times E_{HOMO}$	0.81	0.74	0.86
3	$\ln k_{HO\bullet,OC} = 27.373 + 0.059 \times (\#C) - 0.309 \times (\#acid) - 1.626 \times (\#O:C) + 0.674 \times E_{HOMO} - 0.075 \times HLG$	0.80	0.72	0.85

3.3. Portable measurement of HRSCs of test waters

The $k'_{p,MB}$ values in the UV/H_2O_2 process were measured in a series of SMC (IPA or *p*-CBA) solutions to establish the standard curve (i.e., a linear plot of $1/k'_{p,MB}$ vs. HRSC). Fig. 4a shows that the two standard curves established separately with IPA and *p*-CBA had nearly identical slopes. The slight deviation may be ascribed to the small difference between the photon absorption coefficients of IPA and *p*-CBA at 254 nm. Because the water solubility of *p*-CBA is much lower than that of IPA (ca. 1:5300 at ambient temperature), IPA can cover a much wider range of HRSC. Hence, IPA is a better choice for SMC to simulate the HRSCs of more test waters, although *p*-CBA gives rise to a nearly identical slope of the standard curve.

By measuring the $k'_{p,MB}$ in the UV/H_2O_2 process in a test water, the HRSC of the test water could be obtained by referring to the standard curve (Fig. 1). Fig. 4b shows the $k'_{p,MB}$ and corresponding HRSC values of seven test waters. As expected, a smaller $k'_{p,MB}$ was associated with a higher HRSC (i.e., a stronger competition for HO$^\bullet$). Taking the standard curve established with IPA for example, UP showed the highest $k'_{p,MB}$ (121.5 m^2 einstein^{-1}) and the lowest HRSC (6.54 × 10^3 s^{-1}) among the seven test waters, because it only contained bicarbonate/carbonate species (HCO_3^-/CO_3^{2-}) to compete for HO$^\bullet$. By contrast, the high HRSCs of RW1 (5.91 × 10^5 s^{-1}) and RW2 (5.30 × 10^5 s^{-1}) were attributed to their more complex matrices. The DOC values of RW1 and RW2 were 5.91 and 6.10 mg L^{-1}, respectively, higher than those of other test waters (Table 1). In addition, the HRSCs of SF (5.25 × 10^4 s^{-1}) and PFS/UF (1.06 × 10^5 s^{-1}) were lower than those of RW1 and RW2, respectively, implying a partial removal of HO$^\bullet$-scavenging components in water by the treatment processes applied. In addition, it can be seen that

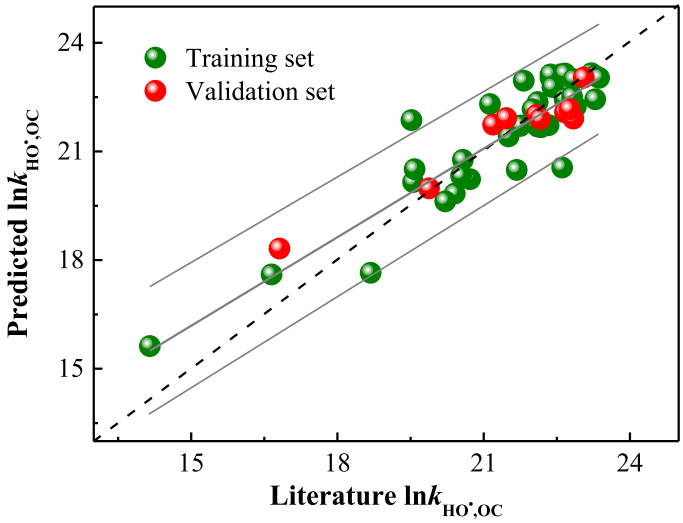

Fig. 3. Comparison of literature and predicted $\ln k_{HO\bullet,OC}$ values of organic compounds in training and validation data sets of QSAR model. Dashed black line: ideal fit; solid gray lines: linear fits with 95% confidence intervals.

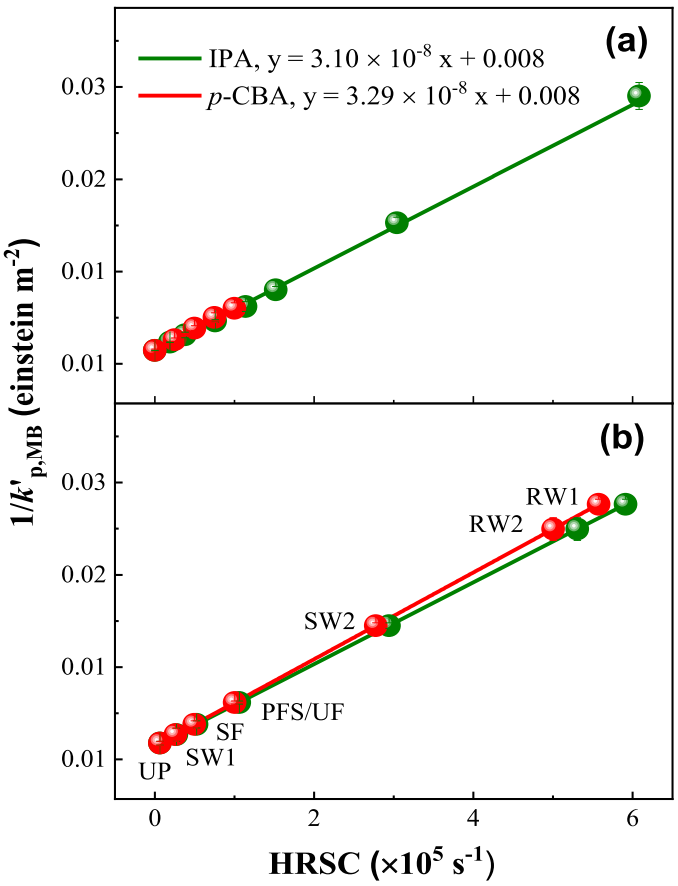

Fig. 4. Plots of $1/k'_{p,MB}$ vs. HRSC: (a) in standard solutions prepared by IPA or *p*-CBA; and (b) in seven test waters. Experimental conditions: $[MB]_0$ = 5.0 mg L^{-1}, $[H_2O_2]_0$ = 25 mg L^{-1}, $[IPA]_0$ = 0 − 320 μM, $[p\text{-CBA}]_0$ = 0 − 20 μM.

the two standard curves separately established with *p*-CBA and IPA led to the similar HRSCs for each test water, albeit with slightly different slopes.

3.4. Prediction of $k'_{p,SMN}$ by MS-PM method and experimental verification

The $r_{HO\bullet}$, $k_{HO\bullet,SMN}$, and HRSC values obtained above were input into the SSA model (i.e., Eq. (4)) to calculate the $[HO^\bullet]_{ss}$ in the seven test waters at various values of $[H_2O_2]_0$ (5–25 mg L^{-1}) and $[SMN]_0$ (0.01−100 μg L^{-1}). As shown in Table 3, the $[HO^\bullet]_{ss}$ increased with increasing $[H_2O_2]_0$ in a certain test water, and varied from 4.5 × 10^{-13} to 4.91 × 10^{-11} M in the seven test waters ($[SMN]_0$ = 100 μg L^{-1}). The highest and lowest $[HO^\bullet]_{ss}$ values were observed in the UP and RW1, respectively, which agrees well with their HRSCs (Fig. 4). In addition, the $[HO^\bullet]_{ss}$ values in the SF and PFS/UF were higher than those in the RW1 and RW2, respectively. Besides, the two standard curves separately established with *p*-CBA and IPA led to similar $[HO^\bullet]_{ss}$ values under the same experimental conditions.

Once the $[HO^\bullet]_{ss}$ was available, the $k'_{i,SMN}$ could be predicted by Eq. (5). Then, the $k'_{p,SMN}$ in each test water was readily calculated by summing up the $k'_{d,SMN}$ and $k'_{i,SMN}$ (i.e., Eq. (1)), as summarized in Table S4. For a certain test water, the predicted $k'_{p,SMN}$ increased with increasing $[H_2O_2]_0$ at a fixed $[SMN]_0$. For all the seven test waters, the predicted $k'_{p,SMN}$ increased with decreasing HRSC (Fig. 4) or increasing $[HO^\bullet]_{ss}$ (Table 3) when $[H_2O_2]_0$ and $[SMN]_0$ were fixed. Again, it is seen that a water matrix with a higher HRSC would consume more $HO^\bullet$, thus leading to a lower $k'_{p,SMN}$.

To verify the predicted values, experiments were further conducted on the MFPS to measure the $k'_{p,SMN}$ values at $[H_2O_2]_0$ = 5–25 mg L^{-1} and $[SMN]_0$ = 100 μg L^{-1}. Micropollutants are usually present in surface and drinking waters at trace levels (i.e., ng L^{-1} to μg L^{-1}) (Luo et al., 2014). Here, a relatively high $[SMN]_0$ (i.e., 100 μg L^{-1}) was adopted for the purpose of convenient analysis of water samples without solid phase extraction. As mentioned above, $[SMN]_0$ in the studied range of 0.010−100 μg L^{-1} showed a negligible impact on the predicted $k'_{d,SMN}$ (Table S1) and $r_{HO\bullet}$ (Fig. S4), and eventually a low impact on the predicted $k'_{p,SMN}$ in all test waters except the UP due to its relatively instable HRSCs (Table S4). Fig. 5 manifests a quite good consistency between the measured and predicted $k'_{p,SMN}$ values in the seven test waters. Nevertheless, it is noted that a majority of the predicted $k'_{p,SMN}$ values were lower than the measured ones, implying that the $k_{HO\bullet,SMN}$ (i.e., 7.2 × 10^9 M^{-1} s^{-1}) predicted by the QSAR model was likely to be underestimated. In the data set for establishing the QSAR model, organic compounds with similar functional groups to SMN, such as amoxicillin, penicillin G/V, tryptophan and tyrosine with amine and/or sulfur groups, also had a predicted $k_{HO\bullet,OC}$ lower than the literature one (Table S3).

The $k'_{p,SMN}$ values measured experimentally in the seven test waters were also provided in Table S4, with the relative percent differences (*RPDs*) all below 12%. The relative error (*RE*) between the predicted and measured $k'_{p,SMN}$ values ranged from −48% to 20% in the seven test waters. A majority of cases showed a negative *RE* value, but the PFS/UF cases showed a positive *RE* value at $[H_2O_2]_0$ = 15 and 25 mg L^{-1}. In the UV/H_2O_2 process, a relatively high residual Fe^{3+} in the PFS/UF (0.34 mg L^{-1}, Table 1) would be reduced to Fe^{2+} under UV irradiation, which further reacted with H_2O_2 to produce reactive radicals (i.e., photo-Fenton process). Meanwhile, Fe^{3+} may also complex with MB to

Table 3
$[HO^\bullet]_{ss}$ values (×10^{-12} M) of seven test waters predicted by IPA and *p*-CBA ($[SMN]_0$ = 100 μg L^{-1}).

Test water	IPA			*p*-CBA		
	$[H_2O_2]_0$ (mg L^{-1})			$[H_2O_2]_0$ (mg L^{-1})		
	5	15	25	5	15	25
UP	21.7	40.5	49.0	21.8	40.7	49.1
SW1	8.08	19.6	27.3	8.39	20.2	28.1
SW2	0.91	2.65	4.30	0.96	2.81	4.54
RW1	0.45	1.33	2.17	0.48	1.40	2.30
SF	4.64	12.2	18.2	4.86	12.8	18.9
RW2	0.50	1.46	2.39	0.53	1.55	2.53
PFS/UF	2.34	6.70	10.5	2.53	7.04	11.0

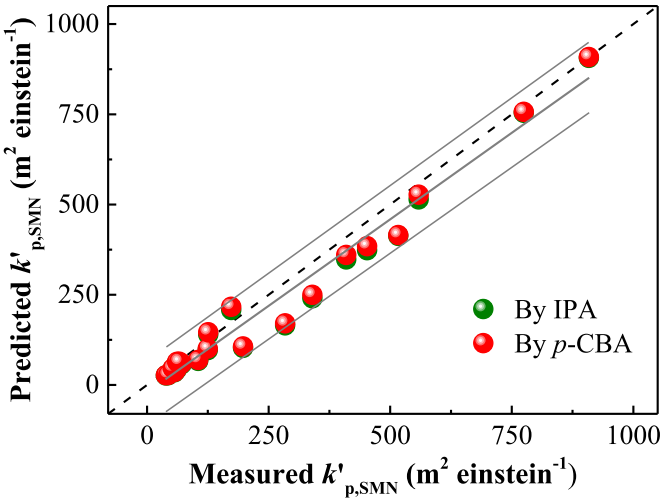

Fig. 5. Comparison of measured and predicted $k'_{p,SMN}$ values in seven test waters. Experimental conditions: $[H_2O_2]_0$ = 5, 15, and 25 mg L^{-1}, $[SMN]_0$ = 100 μg L^{-1}. Dashed black line: ideal fit; solid gray lines: linear fits with 95% confidence intervals.

accelerate the MB degradation (Li et al., 2016b). Hence, the presence of Fe^{3+} in the PFS/UF could induce an overestimation of $k'_{p,SMN}$.

4. Discussion

In general, the predicted $k'_{p,SMN}$ values were lower than the measured ones in the seven test waters, which was primarily attributed to an underestimation of the $k_{HO\bullet,SMN}$ by the QSAR model. In addition, other potential errors may originate from the SSA model and the linear standard curve.

For the QSAR model, in consideration of the cost-benefit ratio of quantum chemical calculation, the molecular conformation was optimized on a local minimum-energy rather than on a global minimum-energy, which may somewhat affect the accuracy of molecular orbital energy calculation (Lee et al., 2015). Furthermore, the data set employed to establish the QSAR model only consisted of 50 organic compounds, which was probably insufficient to achieve reliable statistical analysis results. In the future, the optimization of molecular conformation on a global minimum-energy and a sufficiently large data set may be attempted to improve the QSAR model accuracy.

For the SSA model, only $HO^\bullet$ formed via UV photolysis of H_2O_2 was considered, whereas $HO^\bullet$ and other reactive oxygen species such as singlet oxygen ($^1O_2$) and superoxide anion ($O_2^{\bullet-}$) formed via UV photolysis of DOM were all neglected. This may also cause an underestimation of the predicted $k'_{p,SMN}$.

For the linear standard curve, the $r_{HO\bullet}$ term in the denominator was actually impacted by the UV absorption coefficient (at 254 nm) of a test water, as reflected in Eq. (3). As proposed by Wang et al. (2020), this impact could be significantly alleviated by using a high concentration of probe and a photoreactor with a short optical path-length. In this study, a high concentration of MB (5.0 mg L^{-1}) and the MFPS ($l' = 0.46$ cm) were purposely employed. Fig. S7 shows that the *RE* of $r_{HO\bullet}$ ($\Delta r_{HO\bullet}$), which is defined in Text S2, was below 7.5% for all the seven test waters. Hence, both the accuracy and the range of application were improved for the linear standard curve. Nevertheless, in the future, if the MS-PM method is extended to municipal and industrial wastewaters which have considerably lower UV transmittances than those of surface and drinking waters, the impact of UV absorption coefficient of a test water should be corrected appropriately.

5. Conclusion

This study developed a novel MS-PM method to facilitate prediction of the $k'_{p,MP}$ in the UV/H_2O_2 process. Based on the experimental results, the following conclusions can be drawn:

- An MS-PM method was developed by combining model simulation with portable measurement, which could significantly facilitate prediction of the $k'_{p,MP}$ in the UV/H_2O_2 process. Model simulation was performed with photochemical, $HO^\bullet$ concentration SSA and QSAR models, and portable measurement was conducted on an MFPS to quantify the HRSC of a water matrix.
- Taking SMN as a model micropollutant, the $k'_{p,SMN}$ values predicted by the MS-PM method in seven test waters exhibited a descending order as follows: UP > SW1 > SF > PFS/UF > SW2 > RW2 > RW1. Obviously, the $k'_{p,SMN}$ increased with decreasing HRSC (or increasing $[HO^\bullet]_{ss}$) in the test waters at an identical dose of H_2O_2.
- In general, the predicted $k'_{p,SMN}$ values were lower than the measured ones, which was primarily attributed to an underestimation of the $k_{HO\bullet,SMN}$ by the QSAR model. Although the *RE* of $k'_{p,SMN}$ ranged from −48% to 20% in the seven test waters, the MS-PM method demonstrated a sufficient accuracy if considering its distinct feature, that is, rapid evaluation of the performance of UV-AOPs for micropollutant removal.
- In the future, the MS-PM method can also be extended to other UV-AOPs (e.g., UV/chlorine and UV/persulfate) and other polluted waters (e.g., municipal and industrial wastewaters) after certain modifications. Considering the fact that micropollutants are posing a big challenge to aquatic systems nowadays, this developed method will significantly promote the application of UV-AOPs, especially with the increasingly strict standards of drinking water, municipal wastewater, and industrial wastewater.

Declaration of Competing Interest

The authors declare that they have no known competing financial interests or personal relationships that could have appeared to influence the work reported in this paper.

Data Availability

Data will be made available on request.

Acknowledgments

This work was financially supported by the Ministry of Science and Technology of China (2019YFD1100100), National Natural Science Foundation of China (52091545), and Key Laboratory of Drinking Water Science and Technology (20Z04KLDWST) and Youth Innovation Promotion Association of Chinese Academy of Sciences.

Supplementary materials

Supplementary material associated with this article can be found, in the online version, at doi:10.1016/j.watres.2022.118794.

References

Baeza, C., Knappe, D.R., 2011. Transformation kinetics of biochemically active compounds in low-pressure UV photolysis and UV/H_2O_2 advanced oxidation processes. Water Res. 45 (15), 4531–4543.
Bolton, J.R., Mayor-Smith, I., Linden, K.G., 2015. Rethinking the concepts of fluence (UV dose) and fluence rate: the importance of photon-based units - a systemic review. Photochem. Photobiol. 91 (6), 1252–1262.
Boreen, A.L., Arnold, W.A., McNeill, K., 2005. Triplet-sensitized photodegradation of sulfa drugs containing six-membered heterocyclic groups: identification of an SO_2 extrusion photoproduct. Environ. Sci. Technol. 39 (10), 3630–3638.
Borhani, T.N.G., Saniedanesh, M., Bagheri, M., Lim, J.S., 2016. QSPR prediction of the hydroxyl radical rate constant of water contaminants. Water Res. 98, 344–353.
Buxton, G.V., Greenstock, C.L., Helman, W.P., Ross, A.B., 1988. Critical review of rate constants for reactions of hydrated electrons, hydrogen atoms and hydroxyl radicals (•OH/•O-) in aqueous solution. J. Phys. Chem. Ref. Data 17 (2), 513–886.
Chen, S., Yuan, M.Z., Feng, W.B., Liu, W., Zhang, W., Xu, H.T., Zheng, X.Y., Shen, G.X., Guo, C.X., Wang, L.Q., 2020. Catalytic degradation mechanism of sulfamethazine via photosynergy of monoclinic $BiVO_4$ and microalgae under visible-light irradiation. Water Res. 185, 116220.
Eaton, A.D., Clesceri, L.S., Greenberg, A.E., Franson, M.A.H., 1995. Standard Methods for the Examination of Water and Wastewater, 19th ed. American Public Health Association, Washington DC.
Glaze, W.H., Lay, Y., Kang, J.W., 1995. Advanced oxidation processes-A kinetic model for the oxidation of 1,2-dibromo-3-chloropropane in water by the combination of hydrogen peroxide and UV radiation. Ind. Eng. Chem. Res. 34 (7), 2314–2323.
Goldstein, S., Aschengrau, D., Diamant, Y., Rabani, J., 2007. Photolysis of aqueous H_2O_2: quantum yield and applications for polychromatic UV actinometry in photoreactors. Environ. Sci. Technol. 41 (21), 7486–7490.
Grebel, J.E., Pignatello, J.J., Mitch, W.A., 2010. Effect of halide ions and carbonates on organic contaminant degradation by hydroxyl radical-based advanced oxidation processes in saline waters. Environ. Sci. Technol. 44 (17), 6822–6828.
Hou, L.J., Yin, G.Y., Liu, M., Zhou, J.L., Zheng, Y.L., Gao, J., Zong, H.B., Yang, Y., Gao, L., Tong, C.F., 2015. Effects of sulfamethazine on denitrification and the associated N_2O release in estuarine and coastal sediments. Environ. Sci. Technol. 49 (1), 326–333.
Jin, S.S., Mofidi, A.A., Linden, K.G., 2006. Polychromatic UV fluence measurement using chemical actinometry, biodosimetry, and mathematical techniques. J. Environ. Eng. 132 (8), 831–841.
Jin, X.H., Peldszus, S., Huck, P.M., 2015. Predicting the reaction rate constants of micropollutants with hydroxyl radicals in water using QSPR modeling. Chemosphere 138, 1–9.
Kusic, H., Rasulev, B., Leszczynska, D., Leszczynski, J., Koprivanac, N., 2009. Prediction of rate constants for radical degradation of aromatic pollutants in water matrix: a QSAR study. Chemosphere 75 (8), 1128–1134.

Kwon, M., Kim, S., Jung, Y., Hwang, T.M., Stefan, M.I., Kang, J.W., 2019. The impact of natural variation of OH radical demand of drinking water sources on the optimum operation of the UV/H_2O_2 process. Environ. Sci. Technol. 53 (6), 3177–3186.
Lee, J., von Gunten, U., Kim, J.H., 2020. Persulfate-based advanced oxidation: critical assessment of opportunities and roadblocks. Environ. Sci. Technol. 54 (6), 3064–3081.
Lee, M.J., Zimmermann-Steffens, S.G., Arey, J.S., Fenner, K., von Gunten, U., 2015. Development of prediction models for the reactivity of organic compounds with ozone in aqueous solution by quantum chemical calculations: the role of delocalized and localized molecular orbitals. Environ. Sci. Technol. 49 (16), 9925–9935.
Lee, Y., von Gunten, U., 2012. Quantitative structure-activity relationships (QSARs) for the transformation of organic micropollutants during oxidative water treatment. Water Res. 46 (19), 6177–6195.
Lester, Y., Ferrer, I., Thurman, E.M., Linden, K.G., 2014. Demonstrating sucralose as a monitor of full-scale UV/AOP treatment of trace organic compounds. J. Hazard. Mater. 280, 104–110.
Li, C., Zheng, S.S., Li, T.T., Chen, J.W., Zhou, J.H., Su, L.M., Zhang, Y.N., Crittenden, J.C., Zhu, S.Y., Zhao, Y.H., 2019. Quantitative structure-activity relationship models for predicting reaction rate constants of organic contaminants with hydrated electrons and their mechanistic pathways. Water Res. 151, 468–477.
Li, M.K., Qiang, Z.M., Hou, P., Bolton, J.R., Qu, J.H., Li, P., Wang, C., 2016a. VUV/UV/chlorine as an enhanced advanced oxidation process for organic pollutant removal from water: assessment with a novel mini-fluidic VUV/UV photoreaction system (MVPS). Environ. Sci. Technol. 50 (11), 5849–5856.
Li, M.K., Qiang, Z.M., Pulgarin, C., Kiwi, J., 2016b. Accelerated methylene blue (MB) degradation by Fenton reagent exposed to UV or VUV/UV light in an innovative micro photo-reactor. Appl. Catal. B 187, 83–89.
Luo, X., Wei, X.X., Chen, J.W., Xie, Q., Yang, X.H., Peijnenburg, W.J.G.M., 2019. Rate constants of hydroxyl radicals reaction with different dissociation species of fluoroquinolones and sulfonamides: combined experimental and QSAR studies. Water Res. 166, 115083.
Luo, X., Yang, X.H., Qiao, X.L., Wang, Y., Chen, J.W., Wei, X.X., Peijnenburg, W.J.G.M., 2017. Development of a QSAR model for predicting aqueous reaction rate constants of organic chemicals with hydroxyl radicals. Environ. Sci. Process. Impacts 19 (3), 350–356.
Luo, Y.L., Guo, W.S., Ngo, H.H., Nghiem, L.D., Hai, F.I., Zhang, J., Liang, S., Wang, X.C., 2014. A review on the occurrence of micropollutants in the aquatic environment and their fate and removal during wastewater treatment. Sci. Total Environ. 473, 619–641.
Mezyk, S.P., Neubauer, T.J., Cooper, W.J., Peller, J.R., 2007. Free-radical-induced oxidative and reductive degradation of sulfa drugs in water: absolute kinetics and efficiencies of hydroxyl radical and hydrated electron reactions. J. Phys. Chem. A 111 (37), 9019–9024.
Onstein, P., Stefan, M.I., Bolton, J.R., 1999. Competition kinetics method for the determination of rate constants for the reaction of hydroxyl radicals with organic pollutants using the UV/H_2O_2 advanced oxidation technology: the rate constants for the tert-butyl formate ester and 2,4-dinitrophenol. J. Adv. Oxid. Technol. 4, 231–236.
Rosenfeldt, E.J., Linden, K.G., 2007. The ROH,UV concept to characterize and the model UV/H_2O_2 process in natural waters. Environ. Sci. Technol. 41 (7), 2548–2553.
Schwarzenbach, R.P., Escher, B.I., Fenner, K., Hofstetter, T.B., Johnson, C.A., von Gunten, U., Wehrli, B., 2006. The challenge of micropollutants in aquatic systems. Science 313 (5790), 1072–1077.
Sudhakaran, S., Amy, G.L., 2013. QSAR models for oxidation of organic micropollutants in water based on ozone and hydroxyl radical rate constants and their chemical classification. Water Res. 47 (3), 1111–1122.
Wang, C.J., Rosenfeldt, E., Li, Y., Hofmann, R., 2020. External standard calibration method to measure the hydroxyl radical scavenging capacity of water samples. Environ. Sci. Technol. 54 (3), 1929–1937.
Wang, D., Bolton, J.R., Hofmann, R., 2012. Medium pressure UV combined with chlorine advanced oxidation for trichloroethylene destruction in a model water. Water Res. 46 (15), 4677–4686.
Wang, Y.N., Chen, J.W., Li, X.H., Zhang, S.Y., Qiao, X.L., 2009. Estimation of aqueous-phase reaction rate constants of hydroxyl radical with phenols, alkanes and alcohols. QSAR Comb. Sci. 28 (11–12), 1309–1316.
Wu, J.J., Yang, J.S., Muruganandham, M., Wu, C.C., 2008. The oxidation study of 2-propanol using ozone-based advanced oxidation processes. Sep. Purif. Technol. 62 (1), 39–46.
Wunsch, R., Mayer, C., Plattner, J., Eugster, F., Wulser, R., Gebhardt, J., Huebner, U., Canonica, S., Wintgens, T., von Gunten, U., 2021. Micropollutants as internal probe compounds to assess UV fluence and hydroxyl radical exposure in UV/H_2O_2 treatment. Water Res. 195, 116940.
Xiao, R.Y., Ye, T.T., Wei, Z.S., Luo, S., Yang, Z.H., Spinney, R., 2015. Quantitative structure-activity relationship (QSAR) for the oxidation of trace organic contaminants by sulfate radical. Environ. Sci. Technol. 49 (22), 13394–13402.
Yang, X., Sun, J.L., Fu, W.J., Shang, C., Li, Y., Chen, Y.W., Gan, W.H., Fang, J.Y., 2016. PPCP degradation by UV/chlorine treatment and its impact on DBP formation potential in real waters. Water Res. 98 (7), 309–318.